Pergamon

Computerized Medical Imaging and Graphics, Vol. 19, No. 3, pp. 267–279, 1995
Copyright © 1995 Elsevier Science Ltd
Printed in the USA. All rights reserved
0895-6111/95 $9.50 + .00

0895-6111(95)00007-0

MORPHOLOGY-BASED INTERPOLATION FOR 3D MEDICAL IMAGE RECONSTRUCTION

Jun-Feng Guo,[1] Yuan-Long Cai, and Yu-Ping Wang

Image Processing Center, Xi'an Jiaotong University, Xi'an, Shaanxi Province, People's Republic of China

(*Received 12 January 1995*)

Abstract—Interpolation is an important processing step in 3D reconstruction. A new method, based on mathematical morphology, is presented here to implement the interpolation by means of a combined operation of weighted dilation and erosion. Compared with previously proposed methods, the new approach successfully resolves the interpolation problem when there is no overlapping area between the two objects. In the mean time, it has a wide adaptability and is easy to implement.

Key Words: Interpolation, Three-Dimensional reconstruction, Medical imaging, Computerized tomography, Mathematical morphology

1. INTRODUCTION

Medical imaging, such as computerized tomography (CT), has greatly increased the information available to surgeons, and becomes one of the most important diagnostic methods (1).

With the development of various tomographic medical imaging modalities, there is an urgent need for a three-dimensional (3D) object to be reconstructed from a series of two-dimensional (2D) slices. In the past 10 yr, reconstructing 3D objects on computer from their 2D serial sections is one of the most active research fields (2–7). Major applications of this technique can be found in the study of the biological specimens (8), the study of the structural and morphological characteristics of organs in biomedical sciences (9, 10), radiation treatment planning, surgical planning (11–15), etc.

In medical 3D imaging, the main objectives are to visualize, manipulate, and quantitatively analyze 3D human tissues and organs (16). Its chief task is to build accurately a 3D array consisting of cubic voxels from 2D serial cross-section images. However, the spacing between the slices is typically much greater than (even 5–10 times) the size of a pixel within the slice (1, 17). Therefore, establishing some kind of interpolation between the slices is of vital importance for 3D reconstruction.

Object interpolation is an important class of interpolation method (16, 18–22), which first segments the object of interest to produce a binary image, and then to interpolate this binary image. Two typical object interpolation methods are *Dynamic elastic interpolation* and *Shape-based interpolation*.

Dynamic elastic interpolation (18, 19) comes from elastic matching proposed by Burr (23, 24). The essential idea of dynamic elastic interpolation is to identify a force field acting on one contour and try to distort it so that it looks like the other contour. This method has a wide adaptability whereas the complicated implementation and the computing effort involved prevent it from extensive practical application.

Shape-based interpolation (16, 20) comes from numerical analysis (25). Raya and Udupa adapted this technique to 3D medical image processing (16). Herman, Zheng, and Bucholtz improved the performance of shape-based interpolation by using a distance function that approximates the Euclidean distance more closely (20). Shape-based interpolation first converts the binary images into a new kind of gray-level images wherein the gray value of a point represents its shortest distance (positive value if the point lies inside the object and negative value outside) to the boundary of the object within the slice, and then interpolates the gray image. The set of all points with nonnegative values in the interpolated image constitutes the interpolated object (16, 20). It is a practical interpolation method for its easy implementation. However, this method fails to interpolate the slices when there is no overlapping area between the two objects. These cases are common in medical images, such as the slices of skin, thin bones, and other complicated or tiny tissues.

In order to overcome the drawback of the existing interpolation methods, we develop a new kind of interpolation method—morphology-based interpolation. Theoretical analyses and experimental results have demonstrated that describing interpolation as a combined operation of weighted dilation and erosion is reasonable. The present method has a wide adaptability

[1] To whom correspondence should be addressed.

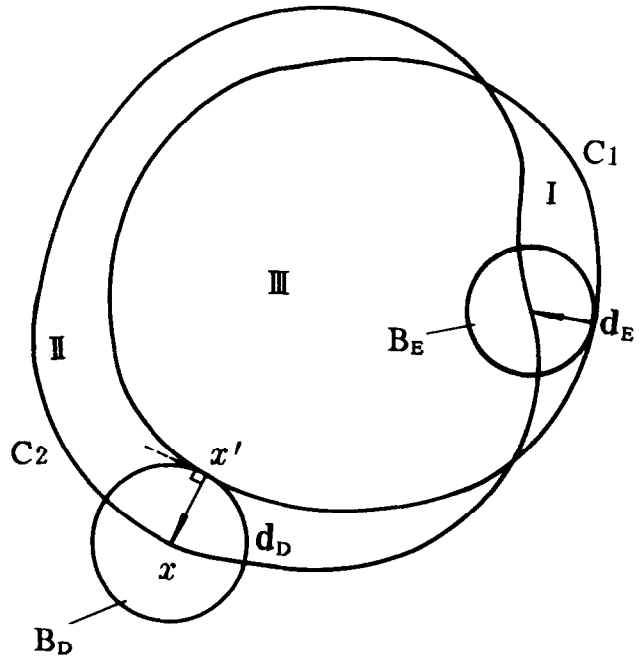

Fig. 1. Morphology-difference image.

and is easy to be implemented. Moreover, describing interpolation problem based on mathematical morphology has presented a new idea and methodology for the study of interpolation.

In the next section, we will describe object interpolation based on morphology. The algorithms and implementational details are presented in Section 3, experimental results in Section 4, and conclusions in Section 5.

2. OBJECT INTERPOLATION BASED ON MORPHOLOGY

Object interpolation between two slices essentially shows the transitional course from one formation to another. Let X_1 and X_2 be object regions in two sequential slices. The aim of interpolation is to generate some new slices between X_1 and X_2 in order to make the change from X_1 to X_2 smooth.

To compare the morphological difference, let us overlap the two slices to get a *morphology-difference image* (*MDI*) between X_1 and X_2, see Fig. 1, where III is the overlapping region of the two objects, I and II are the regions that belong only to X_1 and X_2 respectively. Obviously, region I and II indicate the morphological difference between the two objects X_1 and X_2. In the course of interpolation, by moving the boundary between II and III into region II gradually, region III is enlarged. By a similar process, region I is contracted and disappear at last.

Our approach, as described in the Appendix, is to describe this kind of deformation by weighted dilation and weighted erosion. Under these new concepts, the size of the structuring element (in this paper, we consider structuring element as a circular disk), called weight coefficient, depends on its location. By choosing an appropriate weight coefficient function, X_1 changes to X_2 step by step. The intermediate images are the interpolated layers which we need.

In order to build algorithm easily, move the center of structuring element B to x', as shown in Fig. 2. B_o is the part of B on the side of exterior normal direction of X_1, B_i is the part on the side of interior normal direction. For calculating each of the interpolating image, we now use X_{n+1}, instead of X_2, to indicate target object region, and the $n-1$ interpolate slices, namely $X_2, X_3, \cdots X_n$, between the source object X_1 and the target object X_{n+1} can be computed as follows.

$$X_i = X_{i-1} + \bigcup_{x \in C_1^{i-1}} \frac{\rho_D^{i-1}(x)}{n-i+2} B_o(x) - \bigcup_{x \in C_1^{i-1}} \frac{\rho_E^{i-1}(x)}{n-i+2} B_i(x), \quad 1 < i \le n \tag{1}$$

$$\rho_D^{i-1}(x) = |\mathbf{d}_D^{i-1}(x)|, \quad x \in C_1^{i-1} \tag{2}$$

$$\rho_E^{i-1}(x) = |\mathbf{d}_E^{i-1}(x)|, \quad x \in C_1^{i-1} \tag{3}$$

where n is the spacing between the two original slices, C_1^{i-1} is the object contour of the $(i-1)$th slice, $\rho_D^{i-1}(x)$ and $\rho_E^{i-1}(x)$ are the size of structuring ele-

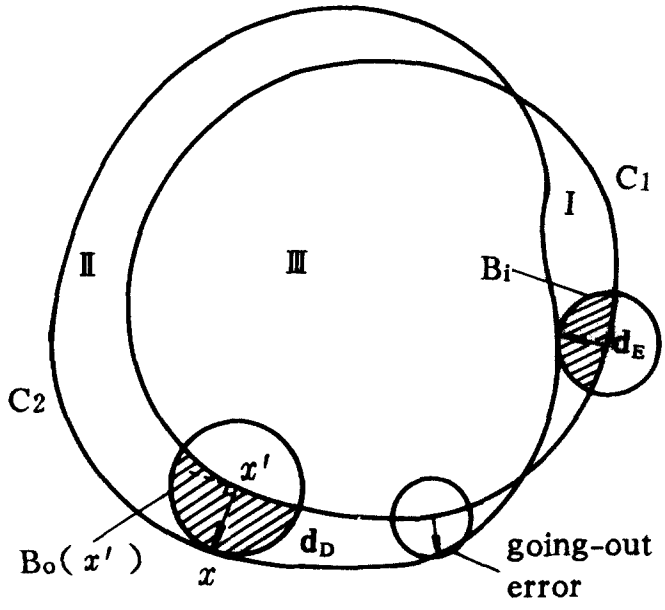

Fig. 2. Schematic diagram of the algorithm.

ments at location x in $(i-1)$th slice for dilation and erosion respectively, and $\mathbf{d}_D^{i-1}(x)$ and $\mathbf{d}_E^{i-1}(x)$ are *morphological difference vectors* (*MDV's*) (see Appendix for detail).

To avoid ambiguity, there should be a unique deformation tendency, dilation or erosion, at each point of the contour C_1. In other words, $\mathbf{d}_D$ and $\mathbf{d}_E$ cannot both have non-zero values at the same position. This can be attained by appropriately choosing source object X_1 and target object X_{n+1} from the two sequential slices as follows:

1. If there is only one connected region in each slice, we choose the slice as X_1 if its region has more contours. As in Fig. 5, the hollow object is a doubly connected region which has two contours and is specified as X_1, and the solid object which is a simply connected region is chosen as X_{n+1}.
2. If one slice has more than one connected regions and the other has only one, the former is specified as X_1 and the latter is taken as X_{n+1}. As in Fig. 6, the slice with three connected regions is considered to be X_1 and the slice with one connected region is considered to be X_{n+1}.
3. If both slices have more than one connected regions, we separate these regions into some relative groups first by classical classification method so that at least one slice in each group has only one connected region. Then we can choose X_1 and X_{n+1} according to the above operation for each group respectively.

3. ALGORITHM

Assume that X_1 and X_{n+1}, specified by the method described in the last section, are source and target object region respectively, we now need to interpolate $n-1$ slices, namely $X_2, X_3, \cdots X_n$, between them.

In order to generate one intermediate slice, there are three major steps.

1. Overlay the source object X_1 and target object X_{n+1} into one image to generate morphological difference image and calculate the exterior normal direction at all contour points of source object X_1.

   Because these two object images are binary images, we can overlap them into one image. In such an image, one byte indicates a pair of pixels where the most significant half byte is used by the source object and the least significant half byte is used by the target object. According to Fig. 1, the pixels in MDI for background, the source-only region I, the target-only region II, and the overlapping region III can be marked by hex as 00, F0, 0F, and FF, respectively.

   The contour of the source object can be easily traced by using eight-neighbour direction chain. We use left-hand rule so that the source object area is always on the left side along the tracing progress. Then for each chain cell, the exterior normal direction can be simply located by rotating the cell direction 90 degrees clockwise. Thus the exterior normal direction at each contour point can be calculated by taking weighted average over several neighbouring chain cell's exterior normal directions.
2. Calculate dilation vector and erosion vector at each contour point of source object, where the erosion vector is calculated only at those contour points at

which the dilation vector is zero. This step will be discussed in detail below.

3. Determine the size of structuring element and implement dilation or erosion.

The radius of the circular disk of structuring element is implied in equation (1), which for dilation is $\rho_D^{i-1}(x)/(n - i + 2)$ and for erosion is $\rho_E^{i-1}(x)/(n - i + 2)$. Once the disk radius has been calculated, we can choose a disk mask image whose radius is equal to the radius calculated. The pixels of the disk are logic '1' in dilation mask and are logic '0' in erosion mask. Based on the principles of Fig. 2, the dilation of X_1 can be done by making OR operation between X_1 and the part of dilation mask which is on the exterior normal side. This operation will be repeated for all source contour points. When this dilation operation is completed, source object X_1 dilates to X_1'. Then the erosion of X_1' will be done for each contour point with non-zero erosion vector by making AND operation between X_1' and the part of erosion mask which is on the interior normal side. When the erosion operation completed, a new interpolated slice X_2 will be generated.

From then on, the other interpolated slices X_3, X_4,$\cdots X_n$ can be generated following the same procedure, by step 1, 2 and 3. For example, when generating X_3, the object X_2 is taken as source object, and when generating X_4, the object X_3 is taken as source object, etc. However the target object is always X_{n+1}. The MDV's should be recomputed for each new slice.

Now step 2 will be detailed as follows. First, we define two terms.

First Continuous Area at searching the next contour: The bar-shaped region from entry point to exit point when the searching point first enters a certain object region in the searching direction, denoted by FCA. Correspondingly, the FCA of object i is denoted by FCA_i.

FCA vector: The current searching vector when the searching point is in FCA, denoted by R_1.

For illustration, some kinds of typical deformation processes are used as examples. There are three pieces of MDI in Fig. 3. Fig. 3a shows that a small ringlike object changes to a big one, in which searching lines 1 and 2 indicate the two kinds of deformation tendency for the two contours of the source object, respectively. Fig. 3b shows that two small solid areas units into a big one, and Fig. 3c shows that a big solid object changes to a small one by shrinking.

The algorithm to determine dilation vector will be discussed first. There are some constraints: the end point of dilation vector should be either on the outer contour of target region II when the searching line encounters region II (Fig. 3a-1), or on the inner contour of overlapping region III when the searching line encounters region III (Fig. 3b). This process is detailed in algorithm SD.

```
Algorithm SD
  begin
    set current searching position S to contour
    point x;
    set current searching vector R as unit exterior
    normal vector at x;
    reset the magnitude of FCA vector to zero;
    while(R < R^D_max) do {
    adjust the position of S;
    if(S ∈ FCA_II) then R_1 ⇐ R;
    else if(S ∈ III) then {
    d_D(x) ⇐ R;
    goto SD_1;
    }
    R ⇐ R + 1;
    }
    d_D(x) ⇐ R_1;
SD_1: set the direction of d_D(x) as the exterior normal
direction at x;
    end
```

where maximum searching radius $R_{\max}^D$ is used as searching limit.

The method to determine erosion vector is similar to the above. There are some constraints: when the target region II (Fig. 3a-2) or overlapping region III (Fig. 3c-2) is in the searching direction, the end point of erosion vector should be on the inner contours of region II or III, otherwise, the end point should be on the outside of the contour of region I (Fig. 3c-1). Details are:

```
Algorithm SE
  begin
    set current searching position S to contour
    point x;
    set current searching vector R as unit interior
    normal vector at x;
    reset the magnitude of FCA vector to zero;
    while(R < R^E_max) do {
      adjust the position of S;
      if(S ∈ FCA_I) then R_1 ⇐ R;
      else if(S ∈ II or S ∈ III) then {
        d_E(x) ⇐ R;
        goto SE_1;
        }
      R ⇐ R + 1;
      }
```

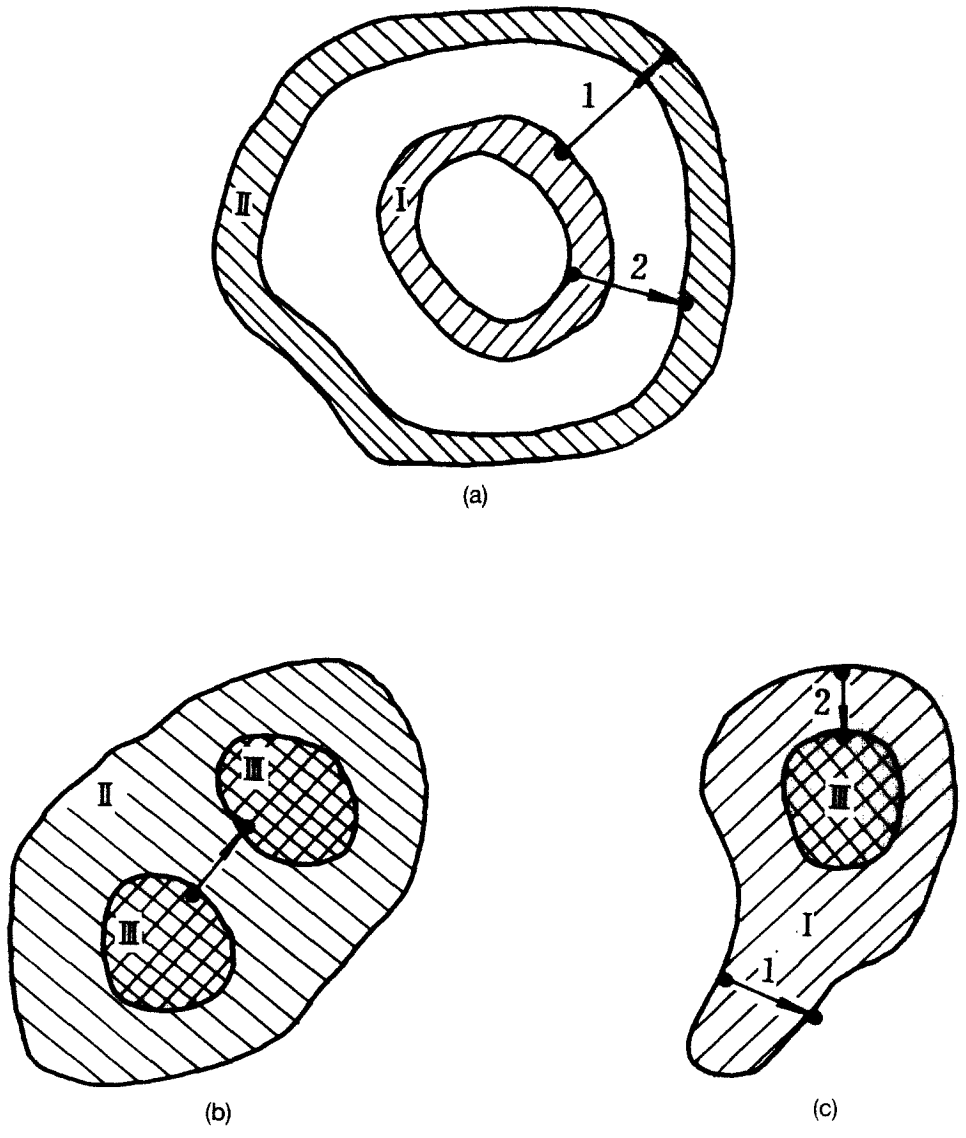

Fig. 3. Diagrams for determining dilation and erosion vector. (See text for descriptions a–c).

$d_E(x) \Leftarrow R_1 + 1$;
SE_1: set the direction of $\mathbf{d}_E(x)$ as the interior normal direction at x;
end

4. EXPERIMENTAL RESULTS

To test the capability of the proposed method, several sets of synthetic and real medical data are used in the experiments. In the meantime, a comparison between the proposed method and shape-based interpolation method has been made.

Figure 4 shows the interpolation performance of a set of ringlike objects with no overlapping area. The experiments demonstrate that the proposed method can give very satisfactory result, but shape-based interpolation method cannot generate integral intermediate contours. The upper left and lower right are two original images, of which the former is the source object image and the latter is the target object image. Image size is 128 × 128. To form a satisfactory 3D display, 62 interpolated slices are generated between the two original slices and the total 64 slices are overlaid to give 3D viewing by means of ray-casting algorithm (26) in Fig. 4c.

Figure 5 demonstrates the interpolation between a hollow object and a solid object. There is another advantage of our method over other existing methods here. Shape-based interpolation and dynamic elastic interpolation methods both fail to deal with this kind of deformation. The image arrangement is the same as Fig. 4.

Figure 6 illustrates the interpolation between two objects, the source object contains more connected re-

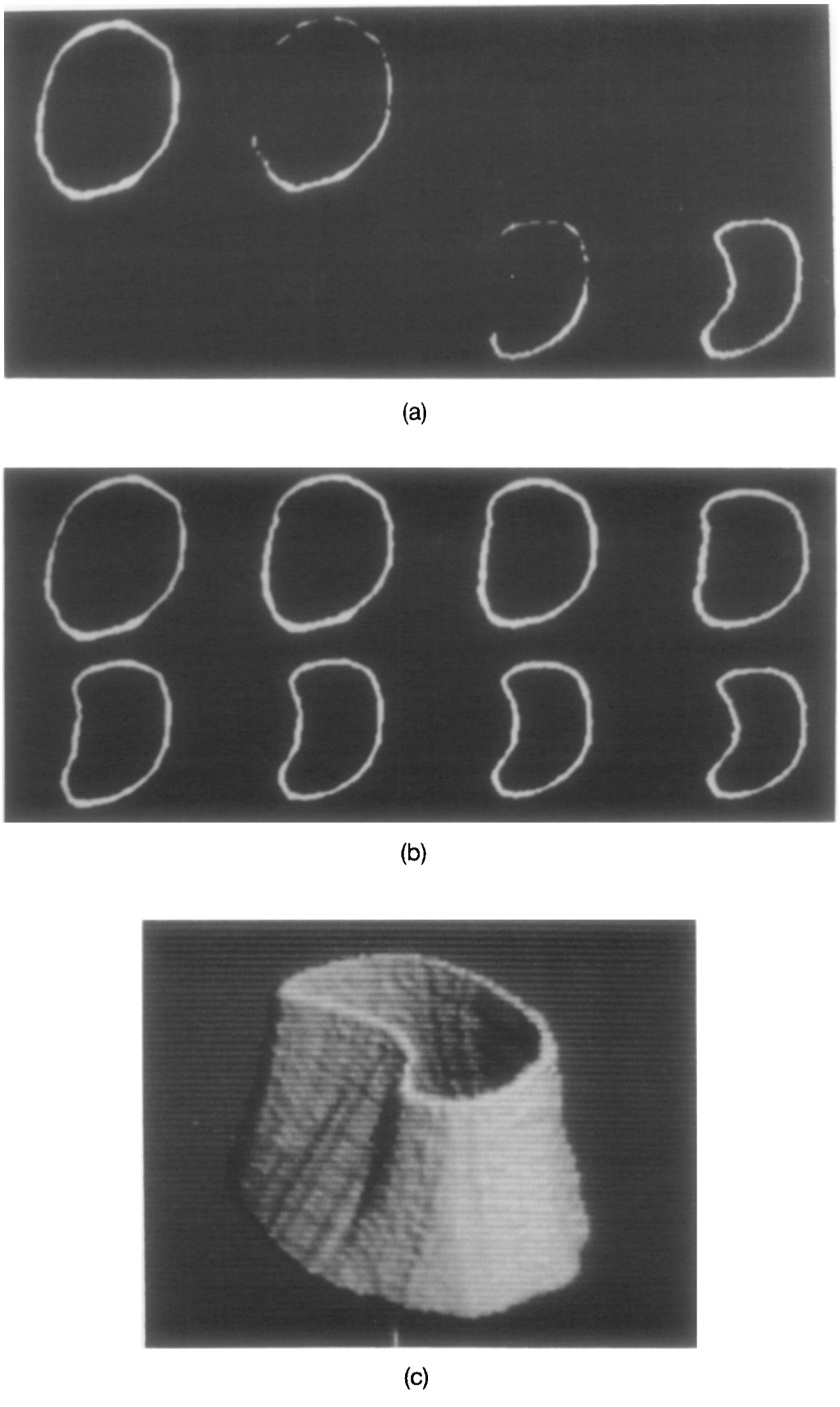

Fig. 4. Interpolation for a set of ringlike objects. (a) The results from shape-based interpolation. The two original images are shown at the upper left and lower right. (b) The results from morphology-based interpolation. (c) 3D display of the object interpolated by morphology-based interpolation using Phong shading model.

gions than the target object. Here, again, the image arrangement is the same as Fig. 4.

To compare the speed for the above three cases of interpolation between the present method and shape-based interpolation, the processing time is recorded respectively in Table 1, where shape-based interpolation method is implemented according to reference (16) and the experiment is made on 33 MHz 486 microcomputer. It can be found out that the time cost of the present method is similar to that of the shape-based interpolation.

Figure 7 shows the interpolation for the head skin

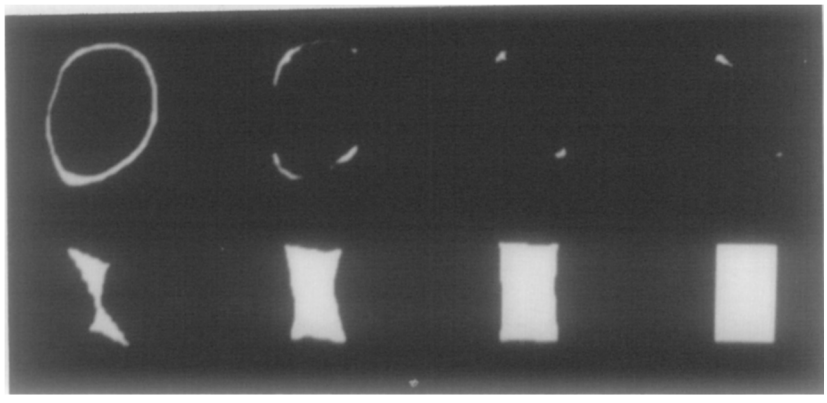

(a)

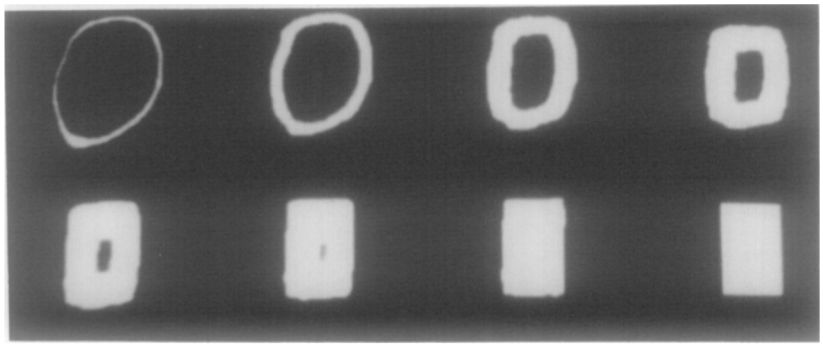

(b)

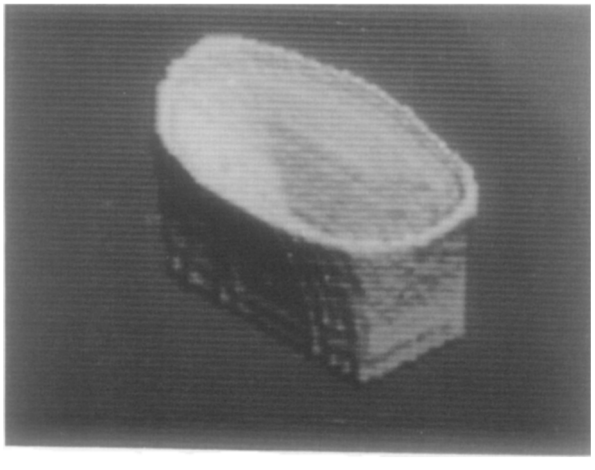

(c)

Fig. 5. Interpolation between a hallow object and a solid object. It is arranged as in Fig. 4. (See text for descriptions a–c).

which is obtained from X-CT by interactive binary segmentation. The original data is 41 slices, where the slice size is 256 × 256 and pixel size within the slice is 1 mm and the slice spacing is 5 mm, five times the pixel size. In order to form voxel data set, four slices are interpolated between two adjacent original slices and a 256 × 256 × 201 voxel data is reconstructed after interpolation. The interpolation is made by using shape-based interpolation and our morphology-based interpolation respectively. The 3D display of these interpolation results are given in Fig. 7. Obviously, the present method gives very satisfactory result, while shape-based interpolation method cannot generate integrated interpolated slices. For clearer observation, a

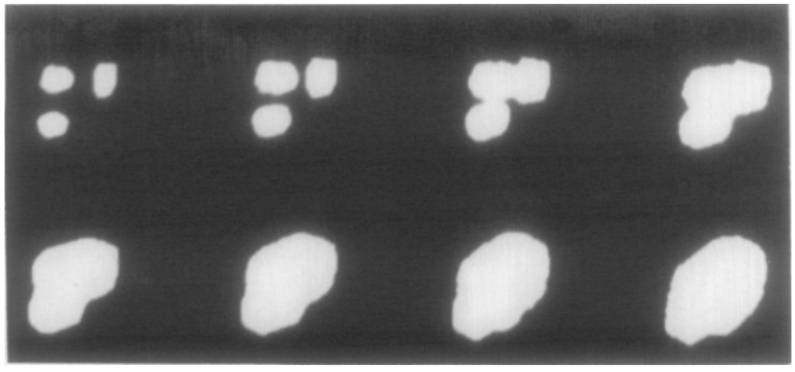

(a)

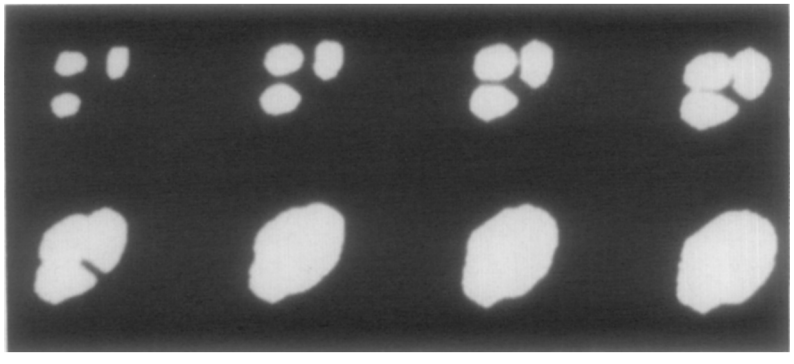

(b)

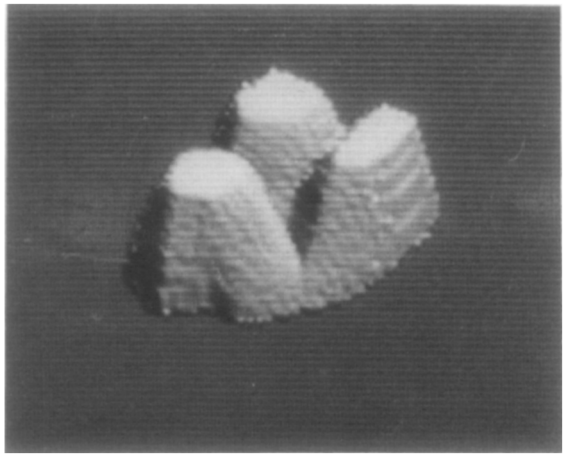

(c)

Fig. 6. Interpolation between an image with three continuous regions and an image with one continuous region. It is arranged as in Fig. 4. (See text for descriptions a–c).

cut-off operation is applied to the 3D display of the present method.

5. CONCLUSION AND DISCUSSION

The essential of interpolation is to extract some common characteristics from adjacent slices, match these characteristics, and gradually change one slice to the other according to the matching information. The result of interpolation is largely determined by matching effectiveness.

Dynamic elastic interpolation, shape-based interpolation, and the present morphology-based interpolation all use the object contour message for matching.

Table 1. Speed comparison between the present method and the shape-based interpolation

Interpolation Method	Morphology-based interpolation	Shape-based Interpolation
Time used for Fig. 4 (s)	9.4	4.2
Time used for Fig. 5 (s)	5.4	10.3
Time used for Fig. 6 (s)	2.6	4.7

Shape-based interpolation method considers only the synthetical result of all the contours, therefore lots of useful information are ignored, so it has the largest error matching probability. Now we assume that the objects are multiply connected regions as shown in Fig. 8. The pixel value in gray-level distance image employed by shape-based interpolation is the shortest distance from all contours. At a certain position, if the two corresponding distance values are determined by two matching contours, the interpolated result is reasonable (see position 1); otherwise an error will occur (see position 2). The most serious error happens when there is no overlapping region. In this case, even a complete interpolated image cannot be generated (see position 3). The other interpolation methods, dynamic elastic interpolation and morphology-based interpolation, consider each contour separately and the above drawbacks are avoided, so these two methods have wider adaptability. Furthermore, morphology-based interpolation, by making use of the whole target object rather than its contour only for characteristics matching, has the least matching error.

Moreover, morphology-based interpolation has more advantages over dynamic elastic interpolation too. First, approximating the contour by polygons is not needed, which is essential in dynamic elastic interpolation method, therefore an object with arbitrarily complicated shape can be accurately processed without leading to new artifacts. Second, dynamic elastic interpolation uses only the contour information for matching, if the object is very thin, the error matching is likely to occur. So it fails to give complete interpolated result for Fig. 7. But the morphology-based interpolation succeeds in avoiding this kind of matching error by using the total target object for matching. Third, the deformation is implemented by morphology operation and complicated computation is eliminated so that the speed of the present method is as fast as that of shape-based interpolation.

However, like the other two methods, the present mathematical model also has difficulty in describing accurately the deformation when the contours contain sharp invaginations or sharp protuberances. As shown in Fig. 9, contour C_1 has a heavy invagination, as a result curve segment ADB cannot be described and left as dead space. Although this kind of deformation cannot be described accurately by the present model, it can still be implemented by the algorithm proposed in section 3 at the cost that the deformation step of curve ADB is large at the beginning interpolated layers compare to that at the end layers. The

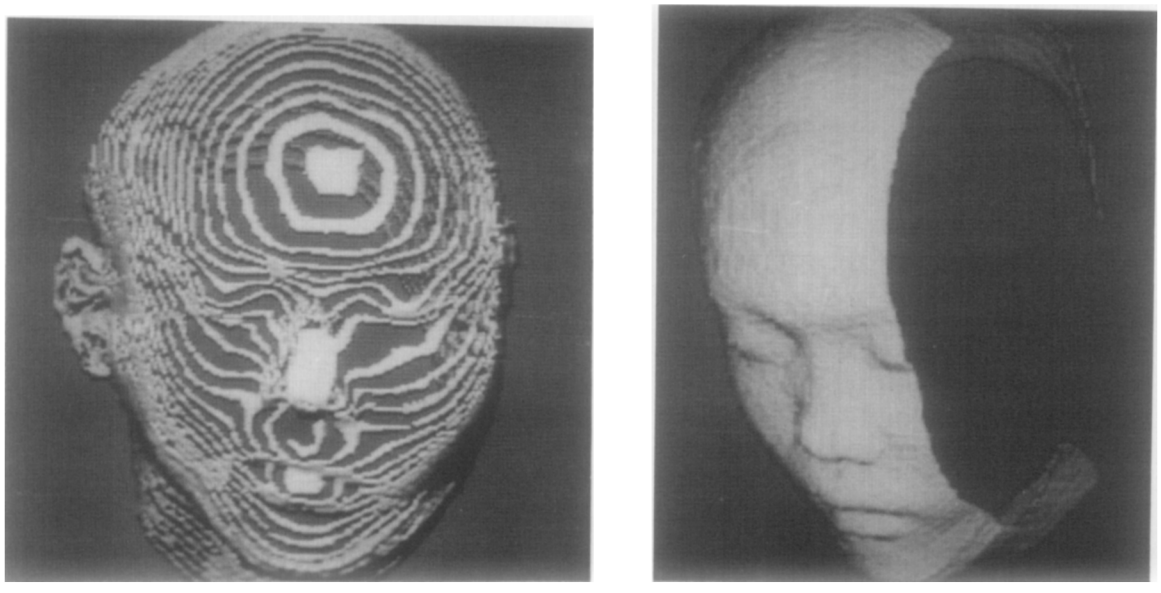

(a) (b)

Fig. 7. 3-D display of the interpolated skin of human head. (a) The result from shape-based interpolation. (b) The result from morphology-based interpolation.

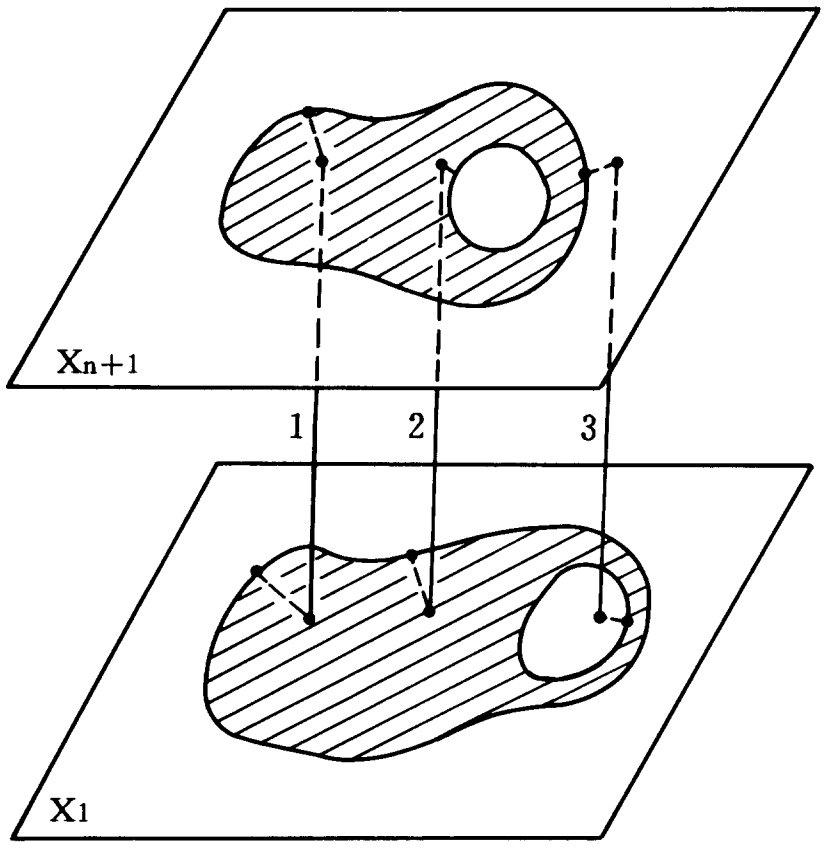

Fig. 8. Schematic diagram of the drawbacks of shape-based interpolation.

interpolated results are usually acceptable although the deforming progress is not as uniform as we expected. Fortunately, these cases occur only in a small percentage

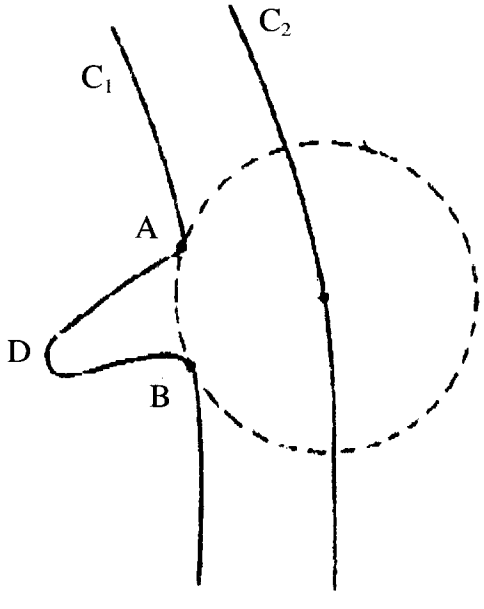

Fig. 9. The limitation of the present model.

in biological tissue and for most of the cases the invaginations or protuberances are not very sharp so that the deformation can be described accurately by the model and be implemented by the algorithm satisfactorily, as shown in Fig. 4. How to describe accurately the deformation when the contour contains heavy invaginations and protuberances by morphological approach is an open problem and needs further investigation.

In this paper, we have presented a methodology and an algorithm to implement interpolation by means of a combined operation of weighted dilation and erosion. It has several advantages over the existing methods. The present approach successfully solves the interpolation problem when there is no overlapping area between the two objects. The interpolation between a hollow object and a solid object can be satisfactorily achieved, so is the interpolation between two objects with unequal number of connected regions. Furthermore, the present algorithm involves less calculation and is easy to be implemented. All the above show that the present method is a practical interpolation approach.

SUMMARY

Interpolation is an important processing step in 3D medical image reconstruction. *Object interpola-*

tion is an important class of interpolation method, two typical methods of which are *Dynamic elastic interpolation* and *Shape-based interpolation*. The former has a wide adaptability, but the complicated implementation and the computing effort involved prevent it from extensive practical application. The latter is practical for its easy implementation, but this method has limited adaptability.

In order to overcome the drawback of the existing methods, based on mathematical morphology, we develop a new kind of interpolation method to implement the interpolation by means of a combined operation of weighted dilation and erosion. Compared with previously proposed methods, the new approach has a wide adaptability and is easy to implement.

There are three major steps in the present method to generate one interpolated slice. First, overlay the source and target objects into one image to generate morphological difference image and calculate the exterior normal direction at all contour points of the source object. Second, at each contour point of the source object, calculate dilation vector and erosion vector. Thus the size of the corresponding structuring element for dilation and erosion can be determined. Finally, by a combined operation of dilation and erosion at the whole source contour, a new interpolated slice can be generated.

To test the capability of the present method, several sets of synthetic and real medical data are used in the experiments. In the meantime, comparison of performance and speed between our method and shape-based interpolation method has been made.

The experiments show that our method has several advantages over the existing methods. The proposed approach successfully resolves the interpolation problem when there is no overlapping area between the two objects. The interpolation between a hollow object and a solid object can be satisfactorily achieved, so is the interpolation between two objects with unequal numbers of connected regions. In the meantime, the present method involves less calculation and is easy to be implemented. All the above show that the present method is a practical interpolation approach.

Acknowledgement—This work is supported by the National Natural Science Foundation of China under Grant 39070305.

REFERENCES

1. Herman, G.T. Special issue on computerized tomography. Proc. IEEE, 71(3):291–435; Mar. 1983.
2. Udupa, J.K.; Herman, G.T., eds. 3D Imaging in medicine. Boca Raton, Fla.: CRC Press; 1991.
3. Batnizky, S.; Price, H.I.; Lee, K.R.; Cook, P.N.; Cook, L.T.; Fritz, S.L.; Dwyer, S.J. III; Watts, C. Three-dimensional computer reconstructions of brain lesions from surface contours provided by computed tomography: a prospectus. Neurosurgery 11:73; 1979.
4. Farrell, E.J.; Zappulla, R.A. Three-dimensional data visualization and biomedical applications. CRC Critical reviews in biomedical engineering. 16(4):323–363; 1989.
5. Woolson, S.T.; Fellingham, L.L.; Dev, P.; Vassiliadis, A. Three dimensional imaging of bone from analysis of computed tomography data. Orthopedics 8:1269; 1985.
6. Herman, G.T.; Liu, H.K. Three-dimensional display of human organs from computed tomograms. CVGIP 9:1; 1979.
7. Nelson, T.R.; Elvins, T.T. Visualization of 3D ultrasound data. IEEE CG&A. 13(6):50–57; 1993.
8. Johnson, E.M.; Capowski, J.J. A system for the three-dimensional reconstruction for biological structures. Comput. Biomed. Res. 16:79–87; 1983.
9. Macagno, E.R.; Levinthal, C.; Sobel, I. Three-dimensional computer reconstruction of neurons and neuronal assemblies. Ann. Rev. Biophys. Bioeng. 8:323–351; 1979.
10. Sobel, I.; Levinthal, C.; Macagno, E.R. Special techniques for the automatic computer reconstruction of neuronal structures. Ann. Rev. Biophys. Bioeng. 9:347–362; 1980.
11. Brewster, L.J.; Trivedi, S.S.; Tuy, H.K.; Udupa, J.K. Interactive surgical planning. IEEE Comput. Graphics Appl. 4:31; Mar. 1984.
12. Kaufman, A.; Yagel, R.; Cohen, D. Intermixing surface and volume rendering. Proceedings of the NATO Advanced Research Workshop on 3D Image in Medicine, Held in Travemünde, Germany, 217–227; June 1990.
13. Bloch, P.; Udupa, J.K. Application of computerized tomography to radiation therapy and surgical planning. Proc. IEEE 71:351–372; Mar. 1983.
14. Vannier, M.W.; Marsh, J.L.; Warren, J.O. Three dimensional computer graphics for craniofacial surgical planning and evaluation. Comput. Graph. 17:263; 1983.
15. Cutting, C.; Grayson, D.D.S.; Bookstein, F.; Fellingham, L.; McCarthy, J.G. Computer-aided planning and evaluation of facial and orthognathic surgery. Comput. Plastic Surg. 13:449–462; 1986.
16. Raya, S.P.; Udupa, J.K. Shape-based interpolation of multidimensional objects. IEEE Trans. Med. Imaging 9(1):32–42; Mar. 1990.
17. Stytz, M.; Frieder, O. Three-dimensional medical imaging modalities: an overview. CRC Critical Reviews in Biomedical Engineering. 18(1):27–54; July 1990.
18. Lin, W.C.; Liang, C.C.; Chen, C.T. Dynamic elastic interpolation for 3D medical image reconstruction from serial cross sections. IEEE Trans. Medical Imaging 7(3):225–232; Sept. 1988.
19. Chen, S.Y.; Lin, W.C.; Liang, C.C.; Chen, C.T. Improvement on dynamic elastic interpolation technique for reconstructing 3D objects from serial cross section. IEEE Trans. Med. Imaging 9(1):71–83; Mar. 1990.
20. Herman, G.T.; Zheng, J.S.; Bucholtz, C.A. Shape-based interpolation. IEEE CG&A. 12:69–79; May 1992.
21. Higgins, W.E.; Morice, C.; Ritman, E.L. New shape-based interpolation technique for three-dimensional images. IEEE Int. Conf. Acoust., Speech, Signal Processing (Albuquerque, NM, April 1990); 1841–1844.
22. Higgins, W.E.; Morice, C.; Ritman, E.L. Shape-based interpolation of tree-like structures in three-dimensional images. IEEE trans. on medical imaging. 12(3):439–450; Sept. 1993.
23. Burr, D.J. A dynamic model for image registration. CVGIP 15:102–112; 1981.
24. Burr, D.J. Elastic matching of line drawings. IEEE Trans. on PAMI PAMI-3:708–713; Nov. 1981.
25. Levin, D. Multidimensional reconstruction by set-valued approximation. IMA J. Numerical Analysis 6:173–184; 1986.
26. Tuy, H.K.; Tuy, L.T. Direct 2-D display of 3D objects. IEEE CG&A 4:29; Oct. 1984.
27. Heijmans, H.J.A.M.; Ronse, C. The algebraic basis of mathe-

matical morphology. I. Dilations and erosions. Comput. Vision Graph. Image Process. 50:245–295; 1990.

About the Author—JUN-FENG GUO received his B.E. degree in telecommunication in 1988 and M.E. degree in communication and electronic system in 1991 in Xi'an Jiaotong University in China. Currently, he is a doctoral student in the Department of Information and Control Engineering, Xi'an Jiaotong University. His research interests include the three-dimensional reconstruction of medical image, image processing, and computer graphics.

About the Author—YUAN-LONG CAI received the B.E. degree in the Department of Electrical Engineering, Jiaotong University, China, in 1951. Currently, he is a professor in the Department of Information and Control Engineering, Xi'an Jiaotong University. His research interests include image processing, pattern recognition, computational vision, and three-dimensional reconstruction of medical image.

About the Author—YU-PING WANG received the B.S. degree in Applied Mathematics from Tianjin University and M.S. degree in Computational Mathematics from Xi'an Jiaotong University at P.R. China in 1990 and 1993, respectively. Currently, he is now pursuing a doctoral programme at the Department of Information and Control Engineering, Xi'an Jiaotong University. He takes interest in wavelet analysis, fractal, and use of spline in image processing.

APPENDIX: MATHEMATICAL MODEL

In order to describe the deformation shown in Fig. 1, we extend the concept of dilation and erosion (27) to weighted dilation and weight erosion.

$$X \boxplus B \triangleq \{x : \rho(x)\check{B}_x \cap X \neq \phi\} \quad (A.1)$$

$$X \boxminus B \triangleq \{x : \rho(x)\check{B}_x \subset X\} \quad (A.2)$$

where $\check{B}_x = \{x - b : b \in B\}$, $\rho(x)\check{B}_x \triangleq \{x - \rho(x)b : b \in B\}$, B is the unit structuring element, $\boxplus$ and $\boxminus$ indicate weighted dilation and weighted erosion respectively. Weight coefficient $\rho(x)$, which depends on its location, indicates the size of the local structuring element.

If the structuring element B is considered as a circular disk with unit radius, then the weight coefficient $\rho(x)$ can be treated as the radius of the local structuring element. Thus the deformation from X_1 to X_2 can be accomplished by choosing an appropriate weight coefficient function. The greater is the local difference between two slices, the larger is the local structuring element.

In order to evaluate quantitatively the difference between X_1 and X_2 in morphology-difference image, see Fig. 1 for example, we introduce a new variable $\mathbf{d}$ called morphology-difference vector (MDV). The direction of $\mathbf{d}$ is defined by the normal direction of contour C_1 at x'. The magnitude of $\mathbf{d}$ is defined as the local difference between X_1 and X_2 along the normal direction. Two types of MDV, morphological dilation vector $\mathbf{d}_D$ and morphological erosion vector $\mathbf{d}_E$, are needed to describe the dilation and erosion deformation. Of course, they are functions of the contour point x'.

By choosing X_1 and X_2 according to the procedure described in Section 2, an advantage that there is a unique deformation tendency, dilation or erosion, at each point of contour C_1 can be obtained. In other words, $\mathbf{d}_D$ and $\mathbf{d}_E$ cannot both have non-zero values at the same position. That is, dilation and erosion can be treated respectively as two independent processes.

For simplicity, the direct deformation course from source object X_1 to target object X_2 without intermediate contour will be first presented.

Let C_1 and C_2 be contours of X_1 and X_2 respectively and let I, II, III be as described in section 2, see Fig. 1. It is clear that $X_1 = \text{I} \cup \text{III}$, $X_2 = \text{II} \cup \text{III}$. Using the concept of weighted dilation and erosion, we see that X_1 can be expanded to $X_1 \cup \text{II}$ by weighted dilation and X_1 can also be shrunk to III by weighted erosion.

Dilation:

$$X_1 \cup \text{II} = X_1 \boxplus B_D = \{x : \rho_D(x)\check{B}_x \cap X_1 \neq \phi\} \quad (A.3)$$

where

$$\rho_D(x) = \begin{cases} \text{Const } \rho, & x \in X_1 \\ |\mathbf{d}_D(x')|, & x \in X_1^C \end{cases} \quad (A.4)$$

and $x' \in C_1$ is chosen so that the normal line of contour C_1 at x' passes through x.

Erosion:

$$\text{III} = X_1 \boxminus B_E = \{x : \rho_E(x)\check{B}_x \subset X_1\} \quad (A.5)$$

where

$$\rho_E(x) = \begin{cases} \text{Const } \rho, & x \in X_1^C \\ |\mathbf{d}_E(x')|, & x \in X_1 \end{cases} \quad (A.6)$$

and, similar to definition (A.4), $x' \in C_1$ is chosen so that the normal line of contour C_1 at x' passes through x.

The deformation course from X_1 to X_2 can be completely described by combining the above two operations. Because $\mathbf{d}_D$ and $\mathbf{d}_E$ cannot both have non-zero values at the same contour point, we have:

$$X_2 = \text{II} \cup \text{III} = (\text{II} \cup X_1) \boxminus B = X_1 \boxplus B_D \boxminus B_E \quad (A.7)$$

However, it is not convenient to build an algorithm directly from equations (A.3) and (A.5) since we need to locate variable x' from x. So we now try to get an approximation for $X_1 \boxplus B_D$ and $X_1 \boxminus B_E$.

As shown in Fig. 2, we move the center of structuring element B to x'. B_o is the part of B on the side

of the exterior normal direction of X_1, B_i is the part on the side of the interior normal direction. Then $X_1 \boxplus B_D$ and $X_1 \boxminus B_E$ can be expressed approximately as:

$$X_1 \boxplus B_D \approx X_1 + \bigcup_{x \in C_1} \rho_D(x) B_n(x) \tag{A.8}$$

$$X_1 \boxminus B_E \approx X_1 - \bigcup_{x \in C_1} \rho_E(x) B_i(x) \tag{A.9}$$

In order to get good approximations, going-out error (see Fig. 2) should be as small as possible. For this reason, we calculate the i-th interpolating image from the deformation of the $(i-1)$th, rather than directly from the original image.

Now we use X_{n+1}, instead of X_2, to indicate target object region. The $n-1$ interpolate slices, X_2, $X_3, \cdots X_n$, between the source object X_1 and the target object X_{n+1} can be computed as follows.

$$\begin{aligned} X_i &= X_{i-1} \boxplus B_D^{i-1} \boxminus B_E^{i-1} \\ &= X_{i-1} + \bigcup_{x \in C_1^{i-1}} \frac{\rho_D^{i-1}(x)}{n-i+2} B_n(x) \\ &\quad - \bigcup_{x \in C_1^{i-1}} \frac{\rho_E^{i-1}(x)}{n-i+2} B_i(x), \quad 1 < i \le n \end{aligned} \tag{A.10}$$

$$\rho_D^{i-1}(x) = |\mathbf{d}_D^{i-1}(x)|, \quad x \in C_1^{i-1} \tag{A.11}$$

$$\rho_E^{i-1}(x) = |\mathbf{d}_E^{i-1}(x)|, \quad x \in C_1^{i-1} \tag{A.12}$$

where n is the distance between the two original slices, C_1^{i-1} is the object contour of the $(i-1)$th slice, and $\mathbf{d}_D^{i-1}(x)$ and $\mathbf{d}_E^{i-1}(x)$ are MDV's between the objects in the $(i-1)$th slice and the $(n+1)$th slice.

Experiments have shown that the approximation is very satisfactory.